Title

Complementary Measurements of Residual Stresses Before and After Base Plate Removal in an Intricate Additively-Manufactured Stainless-Steel Valve Housing

Authors

Clausen, Bjørn
D'Elia, Christopher R
Prime, Michael B
et al.

Publication Date

2020-12-01

DOI

10.1016/j.addma.2020.101555

LA-UR-19-29442

Complementary Measurements of Residual Stresses Before and After Base Plate Removal in an Intricate Additively-Manufactured Stainless-Steel Valve Housing

Bjørn Clausen[1*], Christopher R. D'Elia[2], Michael B. Prime[3], Michael R. Hill[2], Joseph E. Bishop[4], Kyle L. Johnson[4], Bradley H. Jared[5], Kyle M. Allen[6], Dorian K. Balch[7], Allen Roach[5] and Donald W. Brown[1]

[1]MST-8, Los Alamos National Laboratory, Los Alamos, NM 87545, USA
[2]Mechanical and Aerospace Engineering, University of California, Davis, CA 95616, USA
[3]E-13, Los Alamos National Laboratory, Los Alamos, NM 87545, USA
[4]Engineering Sciences Center, Sandia National Laboratories, Albuquerque, NM 87185, USA
[5]Material, Physical and Chemical Sciences Center, Sandia National Laboratories, Albuquerque, NM 87185, USA
[6]Defense Technology Engineering Division, Lawrence Livermore National Laboratory, Livermore, CA 94551, USA
[7]Sandia National Laboratories, Livermore, CA 94551, USA
[*]Corresponding author; clausen@lanl.gov.

Submitted to Additive Manufacturing, Oct 2019
Published On-line Aug 2020 https://doi.org/10.1016/j.addma.2020.101555

Abstract.
Residual stress measurements using neutron diffraction and the contour method were performed on a valve housing made from 316L stainless steel powder with intricate three-dimensional internal features using laser powder-bed fusion additive manufacturing. The measurements captured the evolution of the residual stress fields from a state where the valve housing was attached to the base plate to a state where the housing was cut free from the base plate. Making use of this cut, thus making it a non-destructive measurement in this application, the contour method mapped the residual stress component normal to the cut plane (this stress field is completely relieved by cutting) over the whole cut plane, as well as the change in all stresses in the entire housing due to the cut. The non-destructive nature of the neutron diffraction measurements enabled measurements of residual stress at various points in the build prior to cutting and again after cutting. Good agreement was observed between the two measurement techniques, which showed large, tensile build-direction residual stresses in the outer regions of the housing. The contour results showed large changes in multiple stress components upon removal of the build from the base plate in two distinct regions: near the plane where the build was cut free from the base plate and near the internal features that act as stress concentrators. These observations should be useful in understanding the driving mechanisms for builds cracking near the base plate and to identify regions of concern for structural integrity. Neutron diffraction measurements were also used to show the shear stresses near the base plate were significantly lower than normal stresses, an important assumption for the contour method because of the asymmetric cut.

1 Introduction.

Metal additive manufacturing (metal AM) produces parts by selectively melting and solidifying feedstock to build a desired 3D geometry, rather than the more traditional method of removing material from cast or wrought stock [1,2]. Due to localized cycles of rapid heating and cooling, the constraint of the base

plate, and prior molten material, significant levels of strain and stress arise during fabrication and leave residual stresses in the as-built part [3]. The residual stresses can be large, approaching yield strength, resulting in distortion [3,4], premature fracture, [5] and may affect performance during service.

Several studies have reported measurements of the residual stresses in geometrically simple parts produced by AM using both non-destructive and destructive residual stress measurement methods. Ghasri-Khouzania et al. [6] used neutron diffraction (ND) to measure residual stresses in disks made using laser-powder bed fusion (L-PBF) with various support structures. An et al. [7] used ND and numerical modeling to investigate residual stresses in curved shapes made using L-PBF. Rangaswamy et al. [8] used ND and the contour method (CM) to measure residual stress in laser engineered net shaping (LENS™) made blocks. Brown et al. [3] reported residual stress measured by ND in a rectilinear geometry containing a sharp notch (Charpy specimen geometry), and demonstrated how the notch affected the stress profile. Wu et al. [9] used ND to measure residual stresses in flat prism and L-shaped samples made using L-PBF, and also measured distortion. Strantza et al. [10] used incremental slitting (IS) and incremental hole drilling (IHD) to investigate layer-by-layer variations in residual stresses in L-PBF produced blocks. Vrancken et al. [11] used CM to measure residual stresses in compact tension samples produced via L-PBF. Sillars et al. [4] used a mechanical relaxation method and distortion measurements to evaluate the influence of processing parameter on residual stresses of test samples made using L-PBF.

The focus of this paper is the residual stress field in a valve housing built of 316L stainless steel as part of the Sandia National Laboratories “Born Qualified” Laboratory Directed Research and Development (LDRD) program focused on qualifying additively manufactured parts for high-reliability applications. The housing features an intricate internal shape well suited for applying AM, as cutting the internal features via subtractive manufacture is costly and time consuming.

Assessing residual stress in two conditions, first with the housing attached to the base plate, and second with the housing cut free from the base plate, directly supports development and validation of an advanced process model [12] for long term structural integrity evaluation. The work here presents a novel combination of complementary experimental techniques to most effectively measure the residual stress in the two states. First, ND is used to non-destructively measure the stresses with the housing still on the base plate. Second, a CM measurement, normally considered destructive, makes use of the cut that was required to remove the housing from the base plate, rendering the CM measurement non-destructive in this application. This CM measurement provides two distinct sets of stresses. First, it maps the stresses on the cut plane, which can be compared to the ND measurements. Second, it quantifies the change in all stress components throughout the housing caused by base plate removal [13], which could be combined with the initial ND measurements to give the final stresses. The application of CM to determine change stresses has been validated for multiple stress components on the cut plane [14,15] and also for stresses away from the cut [16,17] but usually on simple shaped specimens. Since the housing is such a complicated shape, a second set of ND measurements are taken in the final state to validate the ability of the contour method to determine the change of the stress state.

Having the CM and ND measurements directly comparable on one plane is a key aspect of the measurement plan. The complex internal shape of the housing poses challenges for both ND and CM techniques as significant stress gradients are expected near the internal features. The ND measurements allow for bulk measurements of the 3D stress state at discrete points inside the part with a relatively modest spatial resolution of a few cubic millimeters, e.g. $2 \times 2 \times 2$ mm^3 [18], and thus the results will be an average over a volume that may have significant stress gradients. The CM measurement provides the

normal stress component on a single plane, the result being a continuous two-dimensional map of the stress field rather than a set of values at discrete points [19]. ND and CM are complementary measurement techniques that rely on distinct assumptions. ND assumes that lattice spacings measured directly in grains can be related to macroscopic stress [20], while CM assumes idealized cutting and predominantly elastic deformation when residual stresses are relaxed by cutting [21]. Past work has focused on using the two diverse and complementary stress measurement techniques as cross-validation for each other, providing strong support for model validation and engineering decisions regarding the character of residual stress that results from fabrication [22]. This work extends that goal by using the two techniques in concert to gain information that could not be gained by either individually.

2 Experimental Methods.

2.1 Sample Preparation.

Figure 1a shows an image of the valve housing as mounted for the diffraction measurements; the origin of the adopted coordinate system is indicated. Figure 1b shows a 3D schematic of the housing displaying the internal structure and Figure 1c shows a side view. The valve housing was produced using a metal laser-powder bed fusion machine (3D Systems, ProX 200) at Sandia National Laboratories, operating in an Argon atmosphere using 316L powder purchased from 3D Systems. Powder samples were gathered in accordance with ASTM B215, and the size distribution was calculated from 100,000 particles observed using SEM images with magnifications from 100X to 10000X. The number-based distributions (D^n_{10}, D^n_{50}, and D^n_{90}), calculated to be the particle diameters at which 10%, 50%, and 90% of the particle population by number were smaller [23], were 11.82µm, 18.09µm and 27.91µm, respectively. The part was produced using a scan pattern in which the laser scanned parallel and orthogonal to the long axis of the housing in alternating, successive layers. 103 W of laser power was utilized with a nominal 1400 mm/sec scan velocity, a 50 µm cross feed and a nominal 30 µm layer thickness. The base plate was 316L stainless steel and of size 140 × 140 × 15 mm^3. The housing was 33.02 mm along the build direction with a footprint of 35.56 (L) × 19.05 (T) mm^2.

The housing has three built-in blind holes: two offset horizontal holes and one central vertical hole. The diameters of the holes are not uniform along the length but exhibit features in support of the function of the valve housing, e.g. thread reliefs and other port features. The sample was marked with North (N), East (E), South (S) and West (W) directions on the base plate; N being the direction from the front to the back of the L-PBF machine and E-W being along the powder spreading direction. The spreading of powder takes place in two steps; a roller applies approximately 90 µm thick layer of powder moving from W to E to ensure full coverage, and on the return path from E to W the same roller reduces the layer thickness to the desired 30 µm.

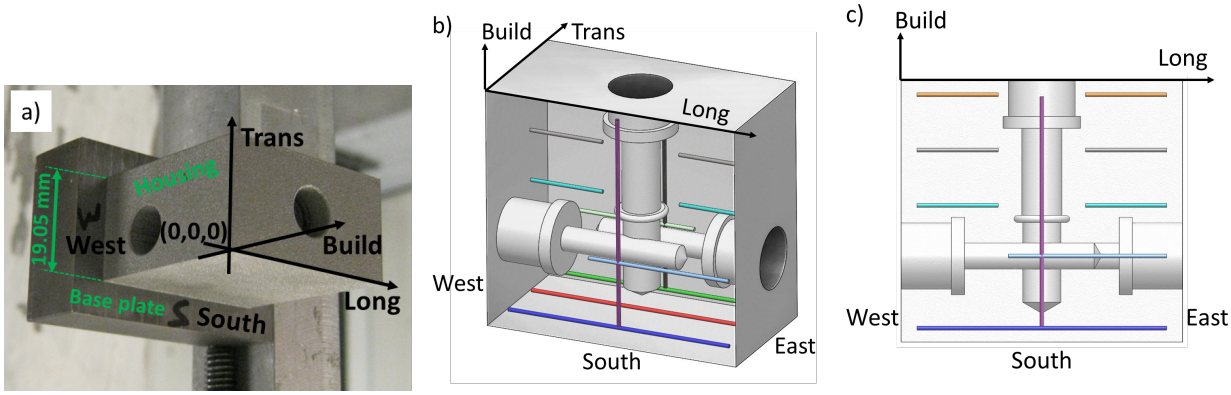

Figure 1: a) Coordinate system shown on the housing, b) and c) 3D schematic and side view of the housing with the colored lines indicating locations of ND measurement shown. The coordinate system is shown with black arrows and text.

The ND residual stress measurements were made along sets of lines defined within the housing, shown in Figures 1b and c): Three horizontal lines 1.75 mm from the intersection of the housing with the base plate. The lower-center line (red) is at the center of the thickness, the lower-south line is 2.3 mm from the South boundary (blue) and the lower-north line (green) is 2.3 mm from the North boundary, respectively; Three horizontal lines at the mid plane of the housing (above the red line) distributed from just above the horizontal holes to close to the top of the housing. The top-center line (orange) is 1.75 mm from the top of the housing, the middle-center line (gray) is 8.75 mm from the top of the housing, and the bottom-center line (turquoise) is 15.75 mm from the top of the housing, respectively. The latter three lines are split in halves by the vertical hole; Two vertical lines at the same center plane as the vertical hole. The vertical-south line (purple) is in-line with the lower-south line (blue) and the vertical-north line (black) is in-line with the lower-north line (green).

The base plate was trimmed to 48.26×31.75 mm^2 (6.35 mm larger than the housing footprint) in order to facilitate ND measurements close to the base plate without asymmetric attenuation of the diffracted neutron beam by the full base plate. Residual strains were measured using ND in two states of the housing: 1) with the trimmed base plate, referred to as *as-built* , and 2) with the base plate cut from the housing, referred to as *parted*, using the terminology introduced in [3]. Wire electrical discharge machining (EDM) was used both to trim the base plate and to part the component from the base plate since EDM using skim cut settings causes minimal machining stress [24]. The final cut that parted the housing from the trimmed base plate was the first step of the CM measurement. This cut used wire EDM and the careful clamping on both sides of the cut typical of CM practice [19,25].

During the ND measurements a coordinate system was defined having its origin at the SW corner of the parallelepiped build away from the base plate as shown in Figure 1. The X (longitudinal or L) and Y (transverse or T) directions lay along the long and short dimensions of the component footprint, respectively; the Z axis is along the build direction (B), see Figure 1.

2.2 Neutron Diffraction.

The ND residual stress measurements were performed using the SMARTS instrument (Spectrometer for Materials Research at Temperature and Stress) at Los Alamos Neutron Science Center (LANSCE) [26]. A detailed description of the instrument has been given elsewhere [26], and here only the salient details of the experimental setup will be described. The pulsed (20Hz) accelerator based source at LANSCE

produces a “white” incident neutron beam with useable neutron wavelength range on the SMARTS instrument from about 0.5 to 7.5Å. The incident beam was defined by motorized boron nitride slits to have a cross section of 2 × 2 mm^2 before impinging on the sample. Two detector banks at +90 and -90 degrees from the incident beam at the sample position were utilized to collect diffracted neutrons. A set of radial collimators with an acceptance length of 2 mm was used to limit the view of the two detector banks; that is to define the resolution along the incident beam. The overlap of the incident neutron beam with the detector view defines a 3D gauge volume of 2 × 2 × 2 mm^3 over which lattice parameter measurements are averaged. The two detector banks simultaneously record independent diffraction patterns with orthogonal scattering vectors [26]. The diffraction scattering vectors, respectively bisecting the incident and diffracted beams associated with the two banks, define the directions along which the lattice strains are measured. By orienting the housing in two orthogonal orientations with respect to the instrument, the lattice strains are determined along three mutually orthogonal directions (scattering vectors), with one of the measurement directions repeated, see Figure 2.

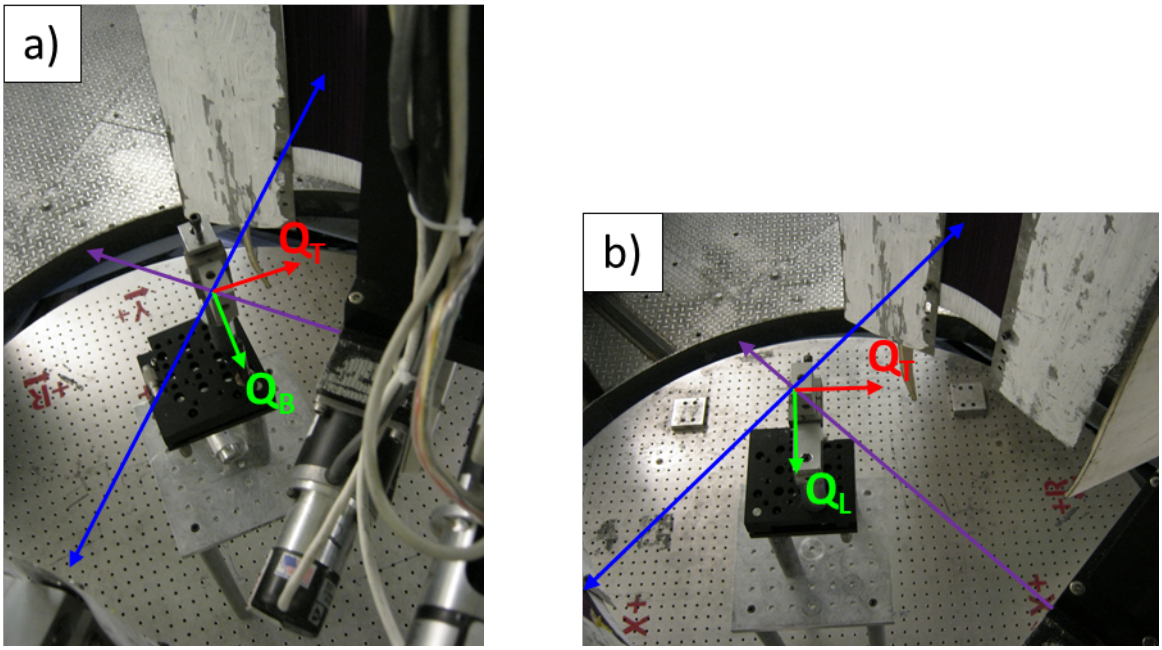

Figure 2: The housing mounted for measurements in SMARTS; a) aligned for measurements along the B and T directions, and b) aligned for measurements along the L and T directions. The purple arrows represent the incident beam, the blue arrows represent the diffracted beams for the two banks, and the red and green arrows represent the scattering vectors for the +90 and -90 degree banks, respectively.

Partial burial of the gauge volume within the material results in significant errors in the measured lattice parameters [18,27]. To ensure the gauge volume is always fully buried within the material, the center of the measurement locations is always chosen to be a minimum of 1.75 mm from any surface, which leaves approximately 0.3 mm of buffer for the $\frac{1}{2}\sqrt{2^2+2^2} = \sqrt{2} \approx 1.41$ mm half-face-diagonal dimension of the gauge volume. Using the computerized theodolites available at SMARTS [26] the positioning accuracy is better than 0.1 mm, depending on the surface finish and available sharp features of the sample.

The lattice parameters were determined using Rietveld refinement [28] of the full diffraction patterns using the GSAS software [29] and the SMARTSware batch refinement routines [30]. The lattice strains were calculated from the change in lattice parameter relative to an assumed stress free reference as:

$$\varepsilon = \frac{a - a_0}{a_0}. \qquad (1)$$

The reference lattice spacing of the steel, a_0, was measured on three 3.5 × 3.5 × 3.5 mm^3 cubes cut from a sister sample at different heights along the build direction, see [31] for guidance on reference measurements. The two states (as-built and parted) were measured in two separate instrument setups as time was needed in-between for the sample to decay to background levels before EDM cutting it off the base plate. Furthermore, the two detectors of the SMARTS instrument are independent measurements, which leads to two sets of two reference lattice parameters as shown in Table 1. The reference cubes were measured in both setups, aligned to the same accuracy as the housing, and the measurements were done in the same directions relative to the build and transverse directions as for the housing. The uncertainties given in Table 1 are the standard deviations over the measurements on the three cubes, and as seen from the low values, there were no differences observed as function of build height or sample direction. There are, however, differences between the states and the banks, which is caused by slight differences in the setups as the instrument was fully reconfigured in-between the measurements to accommodate other users. While these differences between setups influence the absolute values of the reference lattice parameters, they have no impact the strain calculations that are based upon the relative *change* in lattice parameter.

Table 1: Reference lattice parameters for the two states and the two banks.

State	+90 degree bank	Uncertainty	-90 degree bank	Uncertainty
As-built	3.59673	0.00008	3.59754	0.00020
Parted	3.59622	0.00009	3.59841	0.00009

Strain determined from the lattice parameter found through Rietveld refinement of the entire pattern, as compared to single peak determination, have been shown to accurately represent the macroscopic residual strain in the sample [20], and thus appropriate for determining the macroscopic residual stress (Type I stresses) [32]. ND measurements of the shear stresses were also completed on parts of the lower-north/center/south lines for two reasons. First, it is not obvious that the principal stress axes must align with the sample coordinate system as defined in the AM component as is often assumed in ND stress measurement. Secondly, unlike common applications of CM, these measurements depend on an assumption of zero shear stress at the cut interface.

From a mathematical point of view, the measured strains are normal strain components of the full strain tensor projected onto the measurement direction. While a determination of the full stress tensor requires measurement of at least 6 strain components [33], three orthogonal normal stress components can be determined from three measured orthogonal normal strains according to Hooke's law when the material response is isotropic:

$$\sigma_i = \frac{E}{(1+\nu)(1-2\nu)}\Big((1-\nu)\varepsilon_i + \nu\big(\varepsilon_j + \varepsilon_k\big)\Big);\ i,j,k \in B,L,T \qquad (2)$$

where E and ν are Young's modulus and Poisson's ratio for the 316L stainless steel, respectively, see Table 2.

Table 2: Elastic constants used for 316L stainless steel in the stress calculations [34].

Material	Young's modulus (E, GPa)	Poisson's ratio (ν)	Shear modulus (G, GPa)
316L SS	193	0.25	77.2

If the three measured strains are the principal strains, then the measurements represent the full strain tensor and the calculated stress represents the full stress tensor. However, it is not known *a priori*, in general, that the principal axes coincide with the orthogonal measurement directions, and shear strains may be present. Any stress components determined from Eq. 2 can be used for the purpose of validating a process model. However, if the measured results are to be used to predict, for instance, fracture behavior, it is important to find the principal stresses.

Full strain tensor measurements using ND have been reported in the literature [35,36], but most diffraction-based residual stress measurements assume principal directions *a priori*, based on sample geometry, and only these three strains are measured [37,38]. In general, the complex laser path used during the L-PBF process produces localized strain fields from numerous individual melt pools [10], making questionable the assumption that the principle axes align with the external sample boundaries as would be expected in the case of a simple linear weld. In the present work in particular, the complex internal shape of the housing could make the principal directions vary significantly from point to point and to be inconsistent with directions inherited from the overall housing parallelepiped outline and the AM process, i.e. the B, L and T directions. This led to the decision to measure additional strain components in the as-built condition to assess shear strain and stress components at various points in the build, near the base plate, along the lower-north/center/south lines of Figure 1b.

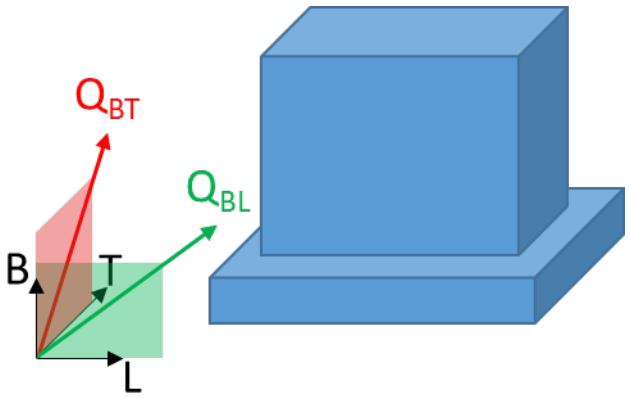

Figure 3: Sketch of the scattering vectors employed to measure the lattice strain components needed to determine the BL and BT shear strains.

To determine two shear stress components, two additional normal strain components were measured with the sample rotated 45° from the original orientation about the transverse and longitudinal axes, so strains were along the build-longitudinal (BL) and build-transverse (BT) directions (ε^{BL} and ε^{BT}), respectively, see Figure 3. The additional strain data were combined with the three original orthogonal

normal strains, along B, L and T, to determine the BL and BT shear strains (γ_{BL} and γ_{BT}) using for instance

$$\gamma_{BL} = 2\varepsilon^{BL} - (\varepsilon_B + \varepsilon_L) \quad (3)$$

Note that superscript was used in equation (3) to identify the measured *normal* strains along the build-longitudinal and build-transverse directions in order not to confuse them with the tensor *shear* strains along the Cartesian directions, e.g. $\varepsilon_{BL} = \gamma_{BL}/2$. Equation (3) is readily found from simple coordinate transformation considerations for a rotation of 45° [39]. The shear stresses are calculated from

$$\tau_{BL} = \gamma_{BL} G \text{ and } \tau_{BT} = \gamma_{BT} G \quad (4)$$

where G is the shear modulus of the 316L stainless steel (see Table 2).

The uncertainty of the strain measurements is propagated from the fitting error of the measured lattice parameters and is generally about ±75 με with maximum of about ±180 με, depending on the neutron path length. The resulting stress uncertainties are generally about ±25 MPa with maximum of about ±50 MPa.

2.3 Contour Method.

Applying the contour method to the cut for removing the base plate yields significant additional information: 1.) A stress map on the plane of the cut and 2.) The stress changes throughout the rest of the housing following the cut. The contour method is a relaxation technique that determines a two-dimensional map of a single component of residual stress acting normal to a plane of interest, while simultaneously determining the *change* in all residual stress components throughout the part [13,21]. This change in stress will be expanded on in the discussion section, and to facilitate this we have defined the Change Stresses (CS) as the difference in stress between the two states, found as the stresses in the parted state minus the stresses in the as-built state. During a typical CM measurement, a prismatic part is sectioned, using wire EDM, along a plane of interest. Usually, the plane of interest is also a plane of geometric symmetry. The sectioning process results in a redistribution of stress in the body (to accommodate the new free surface) which causes distortion of the cut surfaces. Precision metrology equipment is used to measure the cut surface height (i.e. contour) as a function of position in the plane. The stress, normal to the plane of interest, is determined using a linear elastic finite element analysis where the opposite of the cut surface height is applied as a displacement boundary condition to the cut surface. Such an analysis effectively returns the deformed material to its original location, reversing the elastic relaxation and thereby quantifying the change in stress throughout the body [21]. Since the stresses normal to the cut plane are fully relaxed (because of the free surface condition), the change in those stresses are the original residual stresses. Assuming symmetry of the part, a single stress analysis is performed using displacement boundary conditions that are an average of the surface heights measured on each half of the two cut surfaces. Using the average eliminates errors from a non-straight cut path and from shear stress that may exist on the cut plane, and applying smoothing in the form of fitting a surface of bivariate smoothing splines to the measured point clouds minimizes the effect of noise in the data [40].

In the present work, the CM was used to measure residual stress on the plane where the component was cut from the base plate, and so measured the build direction stress component as a function of the longitudinal and transverse position (i.e., $\sigma_B(X, Y)$). A modification to the typical CM analysis was required because the current measurement plane was not a plane of geometric symmetry (i.e. the base

plate has different stiffness than does the built housing). The measured contours on the two sides of the cut were averaged, as is typical for CM. The modification then consisted of applying this averaged contour as displacement boundary conditions in two analyses: one analysis for the baseplate and the other for the build. The measured stress is then the average of results from the two stress analyses. Mahmoudi [41] and our prior work (unpublished) have demonstrated the accuracy of this approach. Because of the geometry asymmetry, the CS throughout the rest of the housing cannot be similarly averaged. Fortunately, the averaged stresses on the cut plane have the information needed to calculate the CS [42]. Therefore, the CS are computed by a third stress analysis, which applied the measured stress field to the cut plane of a new model of the build. The model domain is the valve body after removal from the base plate, the average contour stress field is applied to this domain at the contour plane, and the stress analysis provides the CS throughout the build. It is worth noting that the asymmetry about the cut plane renders the contour measurement susceptible to error from shear stress on the cut plane, an error not present in a typical symmetric CM measurement. Concern over this potential error supported the complementary ND measurements of shear stress near the baseplate.

The uncertainty associated with the CM measurements have previously been determined for a similar material and technique application to have a floor and 95th percentile of about 20 and 40 MPa [43]. Those uncertainties are for the stresses measured on the cut plane. The stress changes decay significantly away from the cut plane per St. Venant's principle, and the uncertainties decay approximately proportionally.

The finite-element-based data reduction of the CM technique was realized using Abaqus CAE Version 6.14 [44]. Linear elastic material behavior was assumed with the material properties given in Table 2. Linear brick elements with incompatible modes were used with local refinement near the contour plane and tetrahedral elements were employed in the more complex areas of the valve housing internals. Tie constraints were placed between the incompatible element faces and the overall solution was calculated using the implicit solver in Abaqus/Standard.

3 Results.

3.1 Neutron diffraction.

Figure 4 shows a comparison of the measured lattice parameters along the build direction on the lower-north/center/south lines (1.75 mm from the base plate) in the as-built and parted states. Comparing the raw measured data in this manner is helpful in gauging repeatability of the absolute determination of the lattice parameter after several intervening months and instrument reconfigures and the appropriateness of the uncertainties based upon the fitting of the data. The axes are held fixed in both plots with the full range of the ordinate representing an elastic strain of just greater than 0.0044. The reference lattice parameters, given in Table 1, are marked with the horizontal dashed lines on the plots. There is significant variation of the build-direction lattice parameter in the as-built state; the lattice parameter is higher than the reference at the ends and lower near the center. Also, the lattice parameter is consistently lower in the central plane of the housing, the lower-center (red) line, then on either side. In contrast, in the parted state the lattice parameters collapse to within a band of about 0.002 Å (~550 $\mu\varepsilon$), with slightly increasing trends close to the end surfaces.

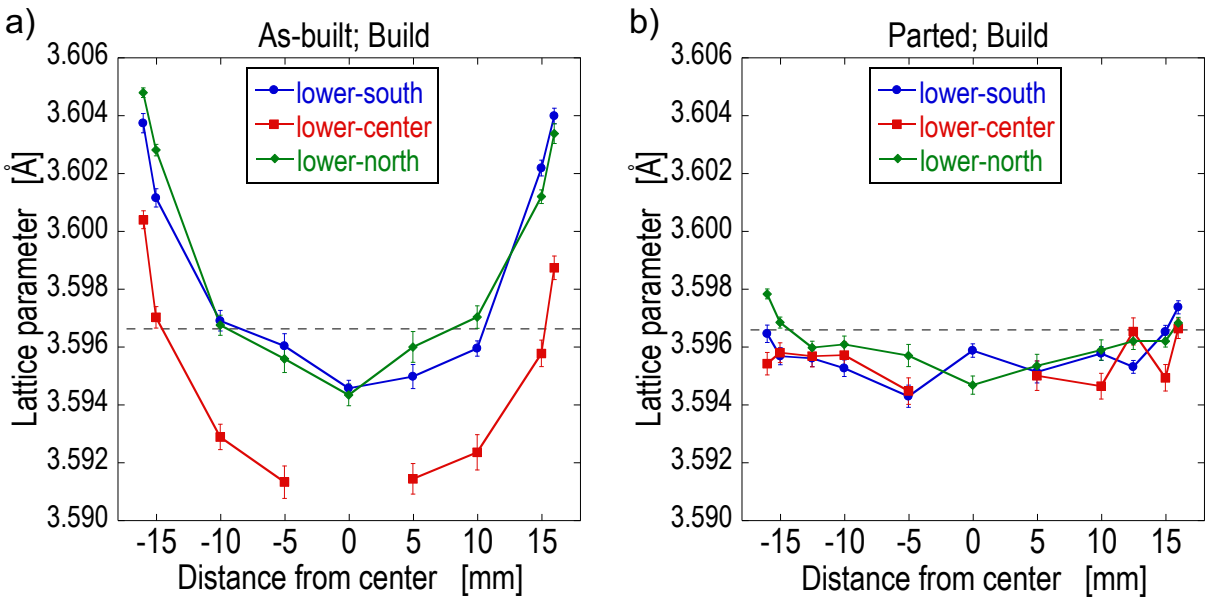

Figure 4: Measured build-direction lattice parameters along the lower-south/center/north lines (blue, red and green lines): a) in the as-built state, and b) in the parted state. The horizontal dashed lines indicate the measured reference stress-free lattice parameter.

A comparison of the measured residual stresses along the B, L and T directions for the as-built and parted states along co-planar lines 1.75 mm from the base plate (lower-north/center/south lines, i.e. blue, red and green, respectively, defined in Figure 1 is shown in Figure 5. The stress uncertainties propagated from the lattice parameter uncertainties are indicated on the plots. In the as-built state, significant tensile build-direction stresses are observed near the E and W sides of the housing with a decrease at the middle. The symmetry between the lines on the N and S sides, (blue and green, respectively) is somewhat surprising given the asymmetry of the horizontal blind holes. The maximum tensile stresses, observed along the B direction, are between 500 and 600 MPa near the corners near the base plate. However, those stresses are rapidly increasing as the end of the measurement range is approached and may continue to do so until the surface is reached. In the middle of the scanned plane, the stresses are compressive and near -200 MPa.

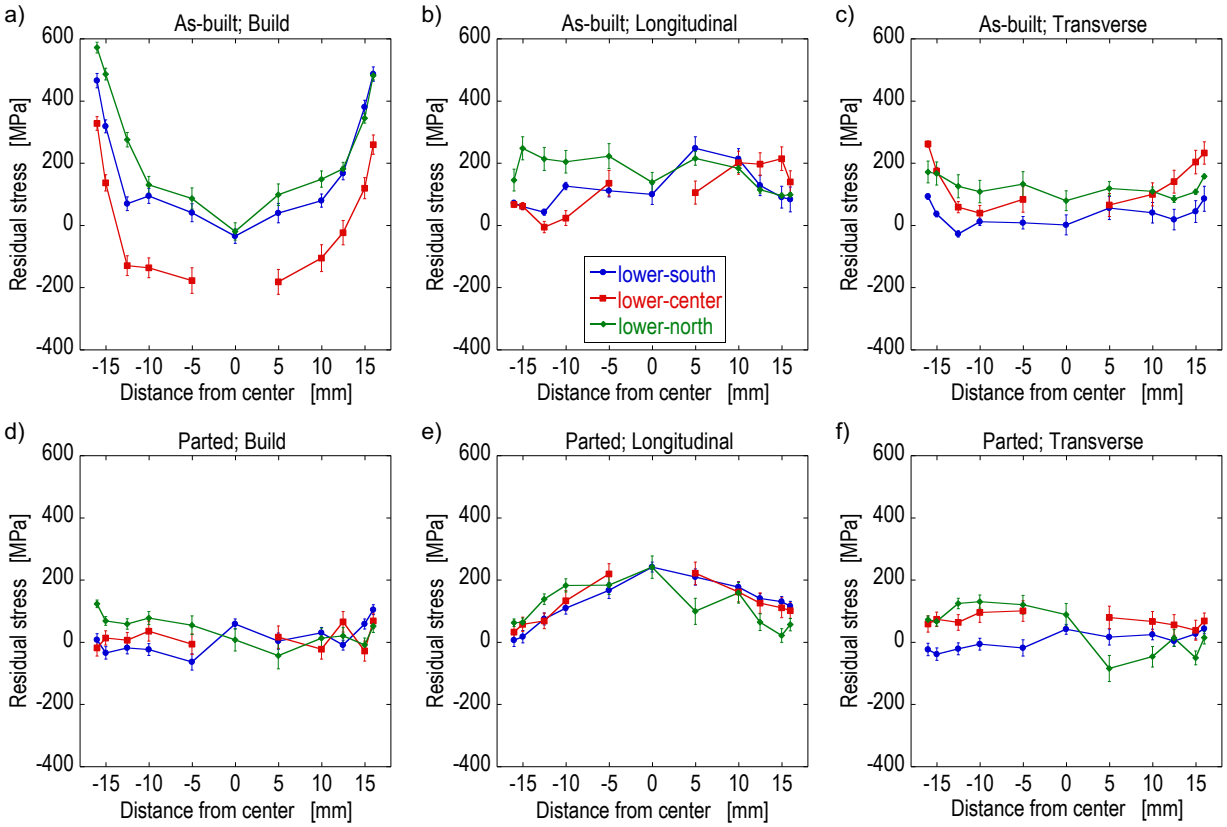

Figure 5: Measured residual stress components in the as-built state along the lower-south/center/north lines (blue, red and green lines): a) build, b) longitudinal, and c) transverse. Measured residual stresses in the parted state along the lower-south/center/north lines: d) build, e) longitudinal, and f) transverse.

In the as-built state near the base plate, the longitudinal and transverse residual stress components are significantly smaller than the build-direction residual stress component. Figure 5b shows a general tensile longitudinal residual stress of up to 200 MPa. This is consistent with cooling of deposited material pulling on the base plate. The longitudinal stresses tend to zero at each end of the lower horizontal lines which is consistent with the nearby free surfaces where the longitudinal stress component must be zero. However, in the as-built state they do not reduce fully to zero at the outermost measurement locations, which could be an indication that the abrupt change in cross section between the housing and the base plate does impose extra constraints that generates further sharp gradients close to the surface and close to the base plate. The longitudinal stress is lower on the west end of the lower-south (blue) line and on the east end of the lower-north (green) line, trends that are consistent with proximity to the laterally offset horizontal holes.

In the parted state, the build-direction stress is near zero at all locations of the lower-north/center/south lines as is expected for a stress normal to a free surface. The longitudinal stresses have decreased to near zero at the ends following parting from the base plate, again as the free surface is approached. They increase to reach 200 MPa near the center of the plane. The transverse stresses are relatively unchanged after parting from the build plate.

The measured shear stresses in the build-longitudinal (BL) and build-transverse (BT) directions on the same plane, 1.75 mm from the base plate, in the as-built state are shown in Figure 6, maintaining the

scale from Figure 3. The shear stresses are relatively small. The maximum value is about 90 MPa which puts the shear stress level at about half of what is observed for the build-direction stresses along these lines in the parted state. This result is significant for the application of the CM to an asymmetric cut where the presence of significant shear stresses along the cut plane introduces a potential source of error [21]. Due to limited beam time allocation the shear measurements were only done on a subset of the locations on the three lower lines; covering one end for all three lines and both ends for the lower-south and lower center lines.

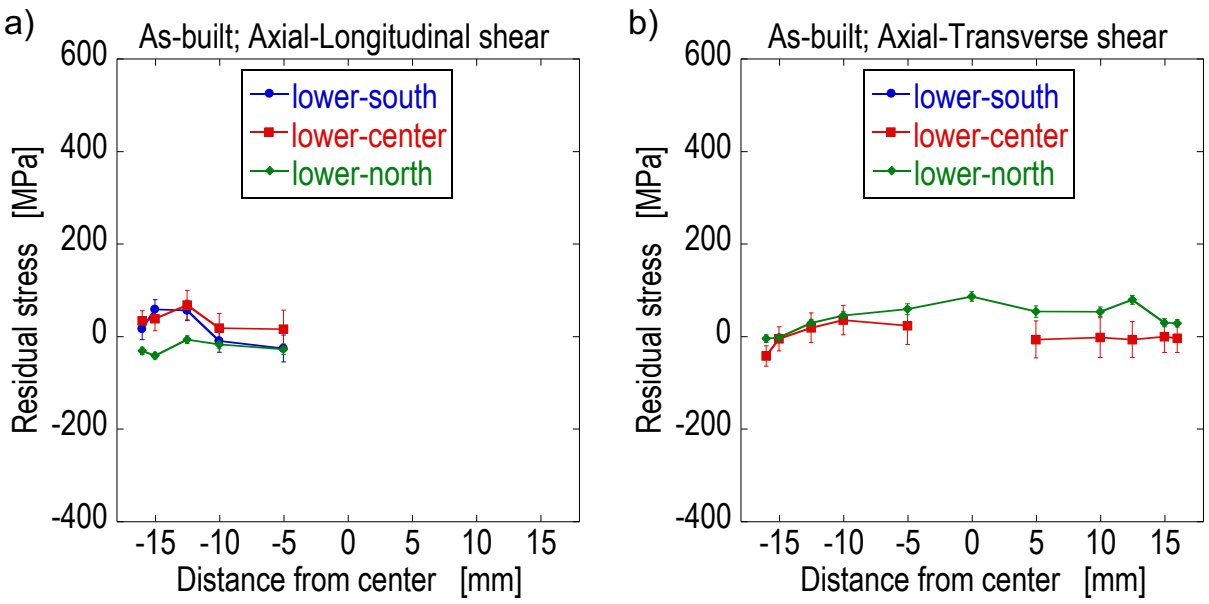

Figure 6: Measured residual shear stresses in the as-built state along the lower-south/center/north lines (blue, red and green lines): a) build-longitudinal (BL) shear, and b) build-transverse (BT) shear (no data for the lower-south line in this direction).

A comparison of the residual stresses in the as-built and parted states along the top/middle/bottom-center (orange, gray and turquoise) lines is shown in Figure 7. In the line closest to the base plate (bottom-center), the trend is similar to the measurement near the base plate (lower-center) in form, which is tensile near the edge and compressive in the center, but reduced in magnitude. The maximum tensile build-direction stresses near the E and W ends are in the 200 to 300 MPa range. The build-direction stresses are generally within uncertainty of zero on the top-center (orange) line, and the longitudinal and transverse stresses on this line closest to the top of the housing are tensile and significant, exceeding 200 MPa at some points. As expected for the locations so far from the base plate, there is minimal change in the observed residual stresses in the top half of the housing following parting from the base plate.

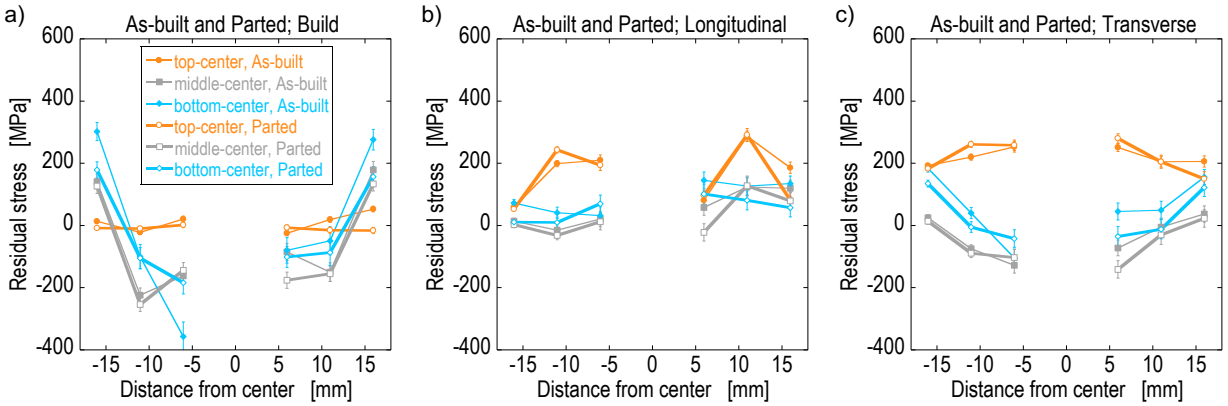

Figure 7: Measured residual stresses in the as-built and parted states along the top/middle/bottom-center lines (orange, gray and turquoise lines): a) build, b) longitudinal, and c) transverse.

A comparison of the observed residual stresses for the as-built and parted states along the south/north-vertical (purple and black) lines is shown in Figure 8. In the as-built state the longitudinal stresses are high near the top of the build, lower in the middle, and slowly increase closer to the base plate. In the parted state near the top of the build, stresses are nearly identical to those in the as-built state. Stress differences between as-built and parted states become larger with increasing distance from the top of the housing. The build-direction and transverse stresses are consistently low in these plots in both as-built and parted states, with those in the parted state being slightly lower. However, this is misleading. The black and purple lines intersect the green and blue lines of Figure 5a) at the center, where they happen to be approximately zero. At another location along the longitudinal direction of the housing, the build direction stresses would be significantly larger. For all stress components in the as-built state, measured stress on the south-vertical (purple) line is more compressive than on the north-vertical (black) line, but in the in the parted state stress on the two lines are more similar.

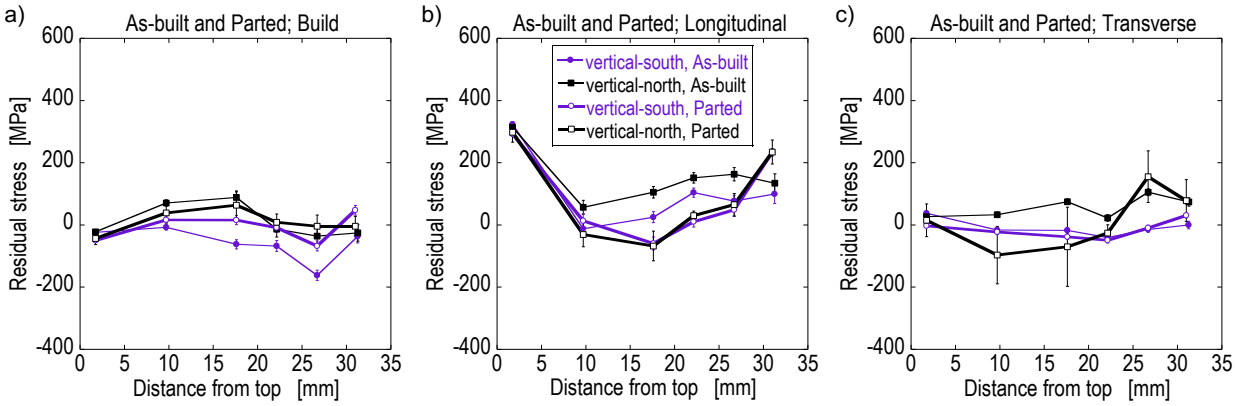

Figure 8: Measured ND residual stresses in the as-built and parted states along the vertical-south and vertical-north lines (purple and black lines): a) build, b) longitudinal, and c) transverse.

3.2 Contour Method.

Figure 9a shows the average measured contour (surface height map) on the plane cut when removing the housing from the base plate; it is an average of the contours of the housing side and the base plate side of the cut. The peak to valley displacement is roughly 0.050mm with the East and West edges

distorting up and away from the base plate. The build-direction stress map on the same plane as determined from the measured contour by the finite element analysis described in section 2.3 for the as-built state is shown in Figure 9b. Significant tensile residual stresses are observed at the perimeter, balanced by a region of compression at the center. At the surface, the build direction stresses are in excess of 400 MPa. The cited yield strength of wrought 316L stainless steel can vary between 200 and 700 MPa depending on the thermo-mechanical heat treatment [45,46] and AM material is typically on the high side of that range [47,48,49], but clearly these stresses are significant compared to the strength of the material. The absolute magnitude of the compressive stresses in the interior of the housing are lower, roughly -250MPa, but over a significantly larger area. There is a slight asymmetry with somewhat higher compressive level towards the west end of the sample. Figure 9c shows a comparison of the CM at the cut surface and the ND measurements along the blue, red and green lines. There is a difference of 1.75 mm along the build direction between the loci of the CM and the ND measurement locations, nevertheless, the two disparate stress measurement techniques produce very similar results, enabling a great deal of confidence in both.

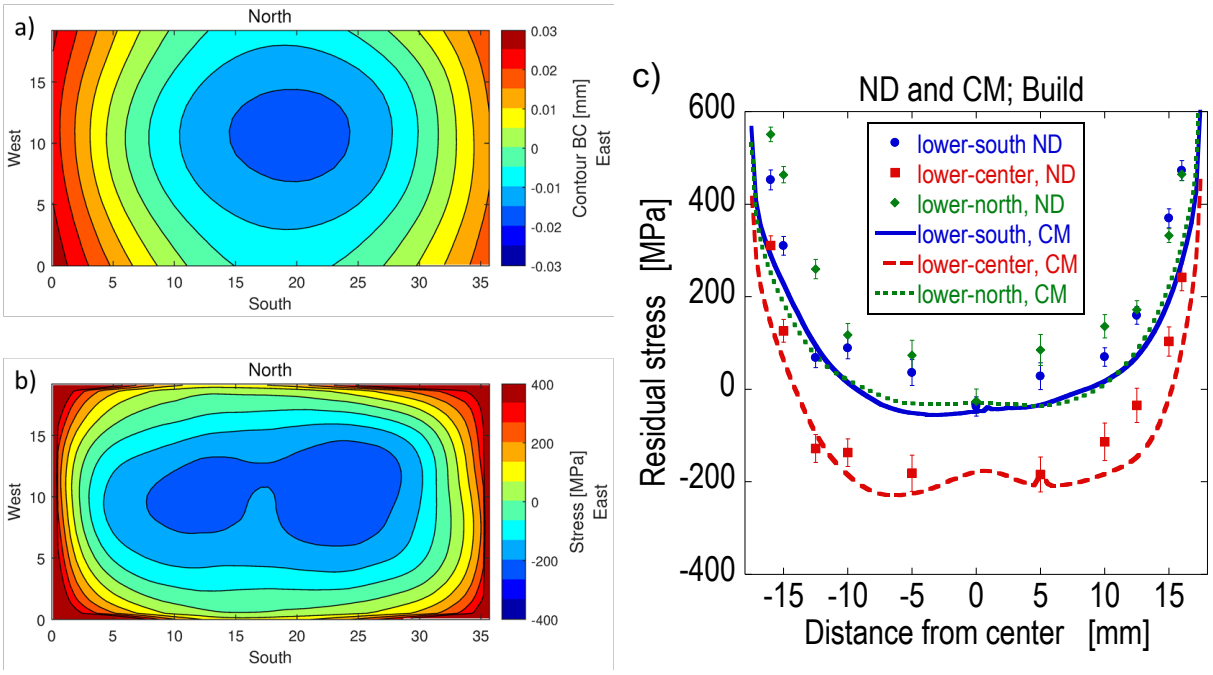

Figure 9: a) Average contour (surface height) measured on the cut surface, b) Average stresses in the Build direction calculated from the measurement in a), and c) a comparison of the measured residual stresses using CM (at the surface) and ND (at the line locations) for the lower-south/center/north lines.

4 Discussion.

Neutron diffraction and the contour method have been used in conjunction previously for the purposes of cross validation of each other [50,51,52]. The added confidence in applying the two distinct measurement techniques to the same or similar samples enhances the experimental results when used for validation of process model simulations. However, the need for removing the as-built AM component from the base plate enables non-destructive coupling of the two techniques to produce results far beyond what either technique can produce standing alone. Once again, this enhances the prospect of utilizing the experimental determination of stress for validating AM process models.

The residual stress state changes significantly when the component is parted from the base plate. The stress relief is necessarily associated with distortion. The build-direction stresses in the as-built state, Figure 5a and Figure 9a, show the characteristic highly tensile regions close to the east and west edges with a dip in the majority of the interior [3,9]. This general stress state with regions of highly tensile build-direction stresses at the sides indicate that the build wants to curl up due to build-generated strains that are restrained by the base plate, causing tensile build-direction stress. Once removed from the base plate, the build distorts (strains) as the build-direction stress is relieved [3,9]. In this work the CM measurement uses the distortion to determine the build-direction residual stress field.

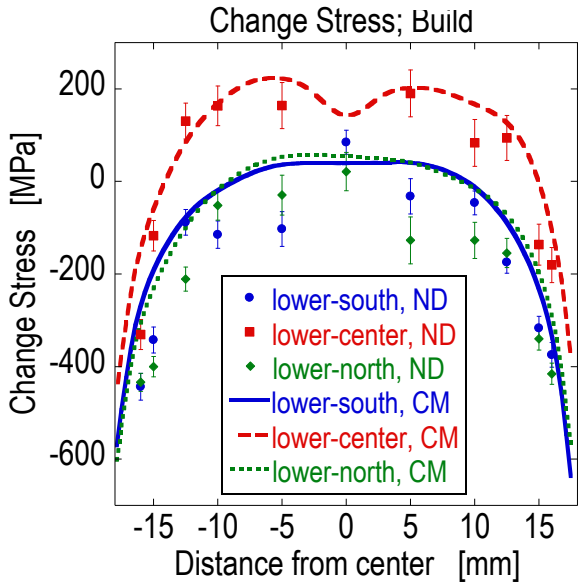

Figure 10: Build direction Change Stress (CS) on the lower-south/center/north (blue, red and green) lines from the ND and CM measurements

The ND and CM data in Figure 9 are not at the same locations: the CM data are inherently at the surface while the ND data are 1.75 mm into the build (to enable measurements both before and after cutting the build free at the same locations), which limits the cross validation of the results. In the following we will use the comparison of the change in stress (or CS as defined in section 2.3) between the two states for a more direct comparison of the two techniques. Bueckner's principle, which is the basis for the CM technique, tells us that the change in stresses over the entire volume of the part being sectioned are uniquely determined by only the stresses fully relaxed on the cut plane [42]. In the present work we can also determine the CS from the ND as we have the ND at identical locations in both states. Hence we can perform direct comparisons of the CS from the two techniques, as shown in Figure 10. The CM data presented in Figure 10 are derived from line plots extracted from the finite element analysis along the measurement lines through the ND gauge volume centroids. Averaging of the CM data over the ND gauge volumes was performed as suggested in [53], but in all cases the difference between the volume averaged value and the line plot value at the center of the gauge volume was less than 2 MPa. Because high tensile stresses at the ends of the blue/red/green lines in the as-built state (Figure 5a) reduce to near zero stress in the parted state (Figure 5b), the CS near the ends of those lines are compressive.

There is good agreement between CS from the CM and ND techniques in Figure 10 , though not quite within uncertainty at all locations. We note consistency of the regions where the lower-south lines are above the lower-north, and vice versa, which are attributed to the offset of the housing internal passages.

As the CM analysis provides the CS in all stress components throughout the housing volume we can present the CS for specific stress components on any plane. Figure 11a shows the longitudinal CS on a virtual sectioning plane containing the south- and north-vertical measurement lines (purple and black). Similarly, Figure 11b shows the build-direction CS on a virtual sectioning plane following the mid-plane of the housing (an example of the transverse direction CS, is not plotted, as they are generally smaller in magnitude). For a simple parallelepiped sample without internal feature the CS is monotonically decaying with distance from the cut surface [21], however, from Figure 11 it is seen that there are local regions of high CS near these internal features.

The largest longitudinal CS (~300MPa) is observed near the cut because of a Poisson effect as the build-direction stress component is fully relieved on the plane of the cut, whereas the transverse direction CS, not plotted, are generally similar in trends, but smaller in magnitude. It is important to note that the stress release must be associated with macroscopic distortion that may take the component out of geometric specification. The build-direction CS is largest near the cut plane and generally decays to smaller magnitudes farther away, as expected by St. Venant's Principle [54]. However, even larger (~400 MPa) build-direction CS are observed near the internal features of the intricate component because of stress concentration effects. A through-hole in a plate has a stress concentration factor of three [55]. The internal features in the housing are holes with intersections and some abrupt shape changes, so they have stress concentrations somewhat larger than three locally in those areas. Large CS near features may lead to later problems in service.

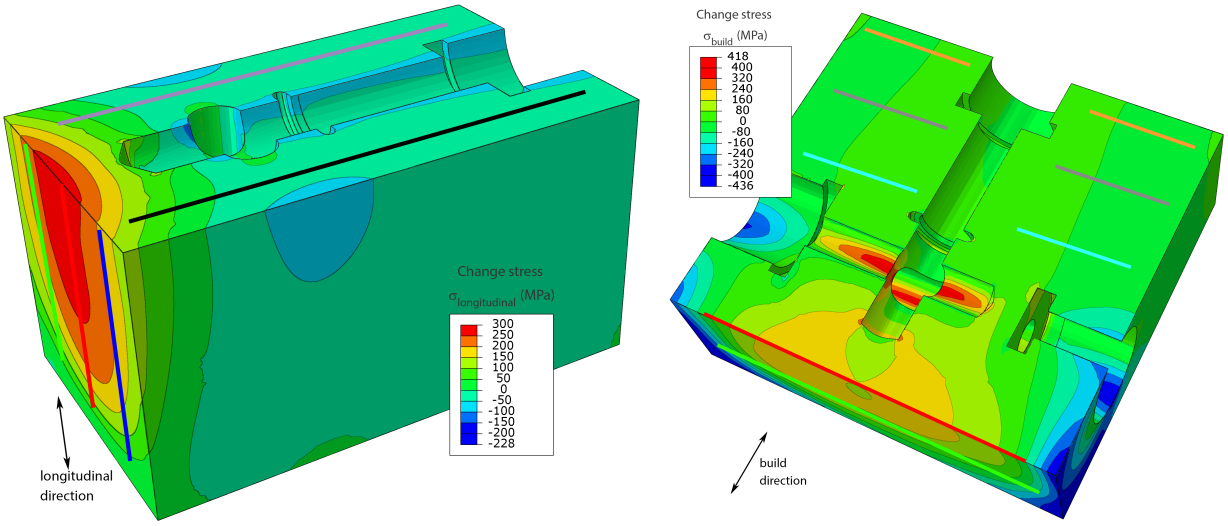

Figure 11. The Change Stress (CS) on two virtual sectioning planes provided by the contour method. Shown on roughly half of the housing where the top surface in each figure is a virtual sectioning plane.

Approximate location of ND scan lines are overlaid for reference. a) longitudinal CS (-200 to 300 MPa colorscale) and b) build direction CS (-400 to 400 MPa colorscale), shown on different sections.

In the present work we employed the ND measurements before and after the parting of the housing from the base plate to validate the use of CM on the parting cut to determine the CS throughout the housing as discussed below. In turn, this means that by applying the CM technique to the parting cut, it is not necessary to perform both sets of ND measurements, as the residual stresses in the as-built part can be determined by combining the CS from the CM measurement with the ND measurements in the parted state. Figure 12 shows a comparison of the residual stress changes along the purple and black lines based upon the ND measurements in the as-built and parted states and the CM results extracted along those paths for all stress components. The significant longitudinal CS observed close to the cut plane where the spatially varying contractions were constrained by neighboring material in the base plate is caused by the Poisson contraction from the build-direction stress relaxation. The transverse CS shows an increase near the base plate similar to the longitudinal stress changes, but at a lower level as it is constrained less due to the smaller lateral dimension of the housing in the transverse direction. The negligible CS in build-direction stress on the vertical-south and vertical-north lines close to the cut plane is a consequence of those paths probing a rare location with near-zero build direction stresses (see Figure 9c at the center, or 0 mm, location), showing that looking at data on only a single path can be quite misleading.

Based on the CM, little or no CS are observed in the upper half of the valve housing following the parting cut, see Figure 11. While an explicit comparison is not shown for brevity, this is consistent with the ND observations that the stresses on the top-, middle- and lower-center lines do not evolve significantly following the cut.

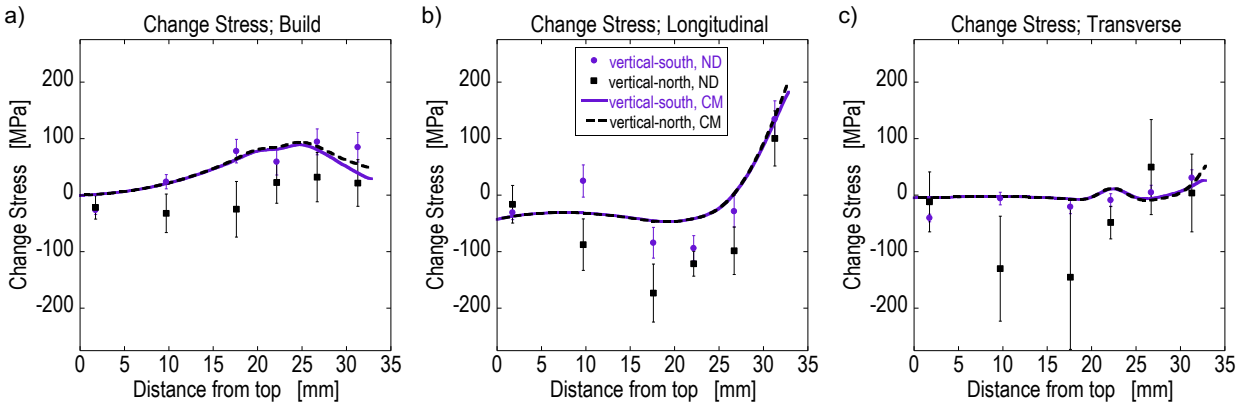

Figure 12: ND and CM Change Stress (CS) along the vertical-south and vertical-north (purple and black) lines: a) build, b) longitudinal, and c) transverse.

The largest CS for all stress components occur in two distinct regions as shown in Figure 11: near the plane of build removal and near geometrical features that act as stress concentrations. For structural integrity purposes, high magnitude stresses are of the most concern. In this work, the ND measurements revealed the CS near the cut plane (Figure 5 and Figure 12b) but missed those near stress concentrations. Given its inherent sampling volume and inability to get data near part surfaces, ND would have difficulty in identifying some of these changes, again highlighting the value of using ND and

CM as complementary residual stress measurement techniques. Note that some locations on the vertical-north line in Figure 12 (and in Figure 8) exhibit increased stress uncertainties caused by insufficient count time employed for these locations. In these locations, the beam path lengths were significantly longer, but the limited beam time allocation did not allow for adding the significant count time needed to decrease the uncertainty, or a sample repositioning that could have alleviated the issue.

The comparison of CS measured by CM and ND generally agree in trends but show scatter in the ND data that may reveal underestimated uncertainty. For example, consider the comparisons in Figure 12. Close to the top, the measurements are so far from the cut plane that by St. Venant's Principle the stress differences must be small. There is therefore no significant uncertainty in those CM results. The ND results disagree outside uncertainty bars with the CM results much more often than would be expected for the one standard deviation uncertainty bars. The most likely explanation is that the reference lattice spacing a_0, which found to be constant within three reference cubes taken at different build heights, in fact varies spatially because of localized effects during the part build. Such variation would be hard to measure without fully destructively sectioning the part and are not captured by the peak fit uncertainties used to estimate stress uncertainties. There are other examples where peak fit uncertainties have been shown to underestimate the total uncertainty for ND, e.g. [56].

5 Conclusions.

Residual strains and stresses in a 316L stainless steel valve housing with intricate three-dimensional internal features built by metal additive manufacturing were measured using neutron diffraction (ND) and the contour method (CM) for two states: with the trimmed base plate (as-built) and removed from the base plate (parted). The ND and CM measurements are in good agreement and due to the distinct assumptions and principles used in the two techniques this provides a very strong validation of both. In the as-built state, the outer perimeter of the valve housing has tensile build-direction residual stresses close to the expected yield strength of as-built material with balancing compression away from the perimeter. This residual stress pattern has been observed for other metal AM parts [3,9] and seems inherent to the L-PBF process.

Residual shear stresses in the valve housing near the base plate were measured using ND in the as-built state and found to be at relatively low levels compared to the measured normal stresses. This is beneficial to both measurement techniques; a typical ND measurement is limited to measuring normal stresses in an assumed principal coordinate system, and in CM measurement the out-of-plane shear stresses are a potential source of error when the cut plane is not a plane of symmetry.

The CM results showed large changes in stress (or CS as defined in section 2.3) upon removal of the build from the base plate in two distinct regions: near the plane where the build was cut free from the base plate and near geometrical features that act as stress concentrations. As expected, the build-direction stresses, those relieved fully at the cut plane, showed the largest CS. However, the longitudinal CS close to the cut were also significant. The internal passages in the housing give rise to some highly localized stresses, evidenced by the large CS in those regions, which could be of concern for structural integrity and deviation from dimensional specifications.

Since the contour method can determine the CS throughout the part from removing the base plate, ND could be used either before or after the base plate removal and the stresses would be known in both states. Performing CM on the parting cut enables experimental determination of regions with large CS that may also be of interest for detailed neutron studies. For the same amount of neutron beam time,

one could more thoroughly look at the final stress state that in the end is the most important for the performance and life time expectation of the part.

The measured residual stresses will be used to validate and support development of L-PBF AM process models in the future.

6 Acknowledgements.

This work has benefited from the use of the Lujan Neutron Scattering Center at LANSCE. Los Alamos National Laboratory is operated by Triad National Security, LLC, for the National Nuclear Security Administration of U.S. Department of Energy (Contract No. 89233218CNA000001). The authors would like to acknowledge funding provided by the Born Qualified Laboratory Directed Research and Development (LDRD) project at Sandia National Laboratories. University of California, Davis was supported by the Sandia Campus Executive program, also through the LDRD office at Sandia. Sandia National Laboratories is a multimission laboratory managed and operated by National Technology & Engineering Solutions of Sandia, LLC, a wholly owned subsidiary of Honeywell International Inc., for the U.S. Department of Energy's National Nuclear Security Administration under contract DE-NA0003525. This paper describes objective technical results and analysis. Any subjective views or opinions that might be expressed in the paper do not necessarily represent the views of the U.S. Department of Energy or the United States Government.

7 References.

[1] D.D. Gu, W. Meiners, K. Wissenbach and R. Poprawe, "Laser Additive Manufacturing of Metallic Components: Materials, Processes and Mechanisms", *Int. Mater. Rev.*, vol. 57(3), pp. 133-164, 2012. http://dx.doi.org/10.1179/1743280411Y.0000000014

[2] J. Li, D. Deng, X. Hou, X. Wang, G. Ma, D. Wu and G. Zhang, "Microstructure and Performance Optimization of Stainless Steel Formed by Laser Additive Manufacturing", *Mat. Sci. Tech.*, vol. 32(12), pp.1223-1230, 2016. http://dx.doi.org/10.1080/02670836.2015.1114774

[3] D.W. Brown, J.D. Bernardin, J.S. Carpenter, B. Clausen, D. Spernjak and J.M. Thompson, "Neutron Diffraction Measurements of Residual Stress in Additively Manufactured Stainless Steel", *Mat. Sci. Eng. A*, vol. 678, pp. 291-298, 2016. http://dx.doi.org/10.1016/j.msea.2016.09.086

[4] S. A. Sillars, C. J. Sutcliffe, A. M. Philo, S. G. R. Brown, J. Sienz and N. P. Lavery, "The three-prong method: a novel assessment of residual stress in laser powder bed fusion", *Virt. Phys. Proto.*, vol. 13(1), pp. 20-25, 2018. http://dx.doi.org/10.1080/17452759.2017.1392682

[5] I. van Zyl, I. Yadroitsava and I. Yadroitsev, "Residual Stress in Ti6Al4V Objects Produced by Direct Metal Laser Sintering", *South African J. Indust. Eng.*, vol. 27(4), pp. 134-141, 2016. http://dx.doi.org/10.7166/27-4-1468

[6] M. Ghasri-Khouzania, H. Peng, R. Rogge, R. Attardo, P. Ostiguy, J. Neidig, R. Billo, D. Hoelzle and M.R. Shankar, "Experimental measurement of residual stress and distortion in additively manufactured stainless steel components with various dimensions", *Mat. Sci. Eng. A*, vol. 707, pp. 689-700, 2017. https://doi.org/10.1016/j.msea.2017.09.108

[7] K. An, L. Yuan, L. Dial, I. Spinelli, A.D. Stoica and Y. Gao, "Neutron residual stress measurement and numerical modeling in a curved thin-walled structure by laser powder bed fusion additive manufacturing", *Materials and Design*, vol. 135, pp. 122-132, 2017. http://dx.doi.org/10.1016/j.matdes.2017.09.018

[8] P. Rangaswamy, M.L. Griffith, M.B. Prime, T.M. Holden, R.B. Rogge, J.M. Edwards and R.J. Sebring, "Residual stresses in LENS® components using neutron diffraction and contour method", *Mat. Sci. Eng. A*, vol. 399, pp.72-83, 2004. http://dx.doi.org/10.1016/j.msea.2005.02.019

[9] A.S. Wu, D.W. Brown, M. Kumar, G.F. Gallegos and W.E. King, “An Experimental Investigation into Additive Manufacturing-Induced Residual Stresses in 316L Stainless Steel”, *Met. Trans. A*, vol. 45(13), pp. 6260-6270, 2014. http://dx.doi.org/10.1007/s11661-014-2549-x

[10] M. Strantza, B. Vrancken, M.B. Prime, C. Truman, M. Rombouts, D. W. Brown, P. Guillaume and D. Van Hemelrijck, “Directional and oscillating residual stress on the mesoscale in additively manufactured Ti-6Al-4V”, *Acta Mater.*, vol. 168, pp. 299-308, 2019. https://doi.org/10.1016/j.actamat.2019.01.050

[11] B. Vrancken, V. Cain, R. Knutsen and J. Van Humbeeck, “Residual stress via the contour method in compact tension specimens produced via selective laser melting”, *Scripta Mater.*, vol. 87, pp.29-32, 2014. http://dx.doi.org/10.1016/j.scriptamat.2014.05.016

[12] K.L. Johnson, T.M. Rodgers, O.D. Underwood, J.D. Madison, K.R. Ford, S.R. Whetten, D.J. Dagel and J.E. Bishop. “Simulation and Experimental Comparison of the Thermo-Mechanical History and 3D Microstructure Evolution of 304L Stainless Steel Tubes Manufactured Using LENS”, *Comp. Mech.*, vol. 61(5), pp 559-574, 2017, https://doi.org/10.1007/s00466-017-1516-y

[13] P. Pagliaro, M.B. Prime, J.S. Robinson, B. Clausen, H. Swenson, M. Steinzig and B. Zuccarello, “Measuring Inaccessible Residual Stresses Using Multiple Methods and Superposition,” *Exp. Mech.,* 51(7), pp. 1123-1134, 2011, https://doi.org/10.1007/s11340-010-9424-5

[14] F. Hosseinzadeh and P.J. Bouchard. “Mapping Multiple Components of the Residual Stress Tensor in a Large P91 Steel Pipe Girth Weld Using a Single Contour Cut”, *Exp. Mech.*, vol. 53, pp. 171-181, 2013. https://doi.org/10.1007/s11340-012-9627-z

[15] M.B. Toparli, M.E. Fitzpatrick and S. Gungor. “Determination of Multiple Near-Surface Residual Stress Components in Laser Peened Aluminum Alloy via the Contour Method”, *Metall. Mater. Trans. A*, vol. 46, pp. 4268-4275, 2015. https://doi.org/10.1007/s11661-015-3026-x

[16] W. Wong and M.R. Hill. “Superposition and Destructive Residual Stress Measurements”, *Exp. Mech.*, vol. 53, pp. 339-344, 2013. https://doi.org/10.1007/s11340-012-9636-y

[17] P. Pagliaro, M.B. Prime, H. Swenson and B. Zuccarello. “Measuring Multiple Residual-Stress Components using the Contour Method and Multiple Cuts”, *Exp. Mech.*, vol. 50, pp. 187-194, 2010. https://doi.org/10.1007/s11340-009-9280-3

[18] “Introduction to the Characterization of Residual Stress by Neutron Diffraction”, P.J. Withers, M.T. Hutchings and T. M. Holden, Chapman and Hall/CRC, 2005.

[19] F. Hosseinzadeh, J. Kowal, and P.J. Bouchard. “Towards good practice guidelines for the contour method of residual stress measurement.” *J. Eng.*, vol. 2014(8), pp. 453-468, 2014. http://dx.doi.org/10.1049/joe.2014.0134

[20] M.R. Daymond, “The Determination of a Continuum Mechanics Equivalent Elastic Strain from the Analysis of Multiple Diffraction Peaks”, *J. Appl. Phys.*, 96(8), 4263-72, 2004. http://dx.doi.org/10.1063/1.1794896

[21] M.B. Prime and A.T. DeWald. “The Contour Method”, Ch. 5 in Practical Residual Stress Measurement Methods, G. S. Schajer (Ed.), 2013, http://dx.doi.org/10.1002/9781118402832.ch5

[22] D. Thibault, P. Bocher, M. Thomas, M. Gharghour and M. Côté, "Residual stress characterization in low transformation temperature 13%Cr-4%Ni stainless steel weld by neutron diffraction and the contour method," *Mat. Sci. Eng. A*, **527**(23):6205-6210, 2010. http://dx.doi.org/10.1016/j.msea.2010.06.035

[23] “Particle Size Characterization”, A. Jillavenkatesa, S.J. Dapkunas, L.-S.H. Lum, NIST Special Publication 960-1, p. 135, 2001. https://doi.org/10.6028/NBS.SP.960-1

[24] W. Cheng, I. Finnie, M. Gremaud and M.B. Prime. “Measurement of near surface residual stresses using electric discharge wire machining”. *J. Eng. Mater. Tech.*, 116(1), 1-7, 1994.

[25] M.B. Prime and A.L. Kastengren, "The Contour Method Cutting Assumption: Error Minimization and Correction," *Exp. Appl. Mech.*, vol. 6, pp. 233-250, 2011. https://doi.org/10.1007/978-1-4419-9792-0_40
[26] M.A.M. Bourke, D.C. Dunand and E. Üstündag, "SMARTS – a Spectrometer for Strain Measurement in Engineering Materials", *Appl. Phys. A*, 74 [Suppl.], S1707–S1709, 2002. http://dx.doi.org/10.1007/s003390201747
[27] X.-L. Wang, Y.D. Wang and J.W. Richardson, "Experimental error caused by sample displacement in time-of-flight neutron diffractometry", *J. Appl. Cryst.*, vol. 35, pp. 533-537, 2002. https://doi.org/10.1107/S0021889802009202
[28] H.M. Rietveld, "A Profile Refinement Method for Nuclear and Magnetic Structures", *J. Appl. Cryst.*, 2, pp. 65-71, 1969. http://dx.doi.org/10.1107/S0021889869006558
[29] R.B. Von Dreele, J.D. Jorgensen and C.G. Windsor, "Rietveld Refinement with Spallation Neutron Powder Diffraction Data", *J. Appl. Cryst.*, 15, 581, 1982. https://doi.org/10.1107/S0021889882012722
[30] "SMARTSware Manual", B. Clausen, LA-UR 04-6581, Los Alamos, NM: Los Alamos National Laboratory, 2004. http://public.lanl.gov/clausen/SMARTSware.html
[31] "Non-destructive testing - Standard test method for determining residual stresses by neutron diffraction, VAMAS-20, ISO/TS 21432:2005(en), 2005. https://www.iso.org/obp/ui/#iso:std:iso:ts:21432:ed-1:v1:en
[32] E. Macherauch and K.H. Kloos, "Bewertung von Eigenspannungen bei quasistatischer und schwingender Werkstoff beanspruchung", *Mat.-wiss. u. Werkstofftech.*, vol. 20, pp. 1-13, 1989. https://doi.org/10.1002/mawe.19890200104
[33] T. Lorentzen T and T. Leffers, "Strain tensor measurements by neutron diffraction". In: Hutchings MT and Krawitz AD (eds) Measurement of residual and applied stress using neutron diffraction, vol. 216 of NATO ANSI Series E, pp. 253-261, 1992. http://dx.doi.org/10.1007%2F978-94-011-2797-4
[34] SS316L Austenitic Stainless Steel Data Sheet, MatWeb LLC, http://matweb.com/search/DataSheet.aspx?MatGUID=9e9ab696974044cab4a7fd83687934eb
[35] H.E. Coules, L.D. Cozzolino, P. Colegrove, S. Ganguly, S.W. Wen and T. Pirling, "Neutron Diffraction Analysis of Complete Residual Stress Tensors in Conventional and Rolled Gas Metal Arc Welds", *Exp. Mech.*, vol. 53, pp. 195-204, 2013. http://dx.doi.org/10.1007/s11340-012-9631-3
[36] J.R. Bunn, D. Penumadu, X. Lou and C.R. Hubbard, "Effect of Multi-Axial Loading on Residual Strain Tensor for 12L14 Steel Alloy", *Met. Trans. A*, vol. 45(9), pp. 3806-3813, 2014. http://dx.doi.org/10.1007/s11661-014-2355-5
[37] D.W. Brown, J.D. Bernardin, J.S. Carpenter, B. Clausen, D. Spernjak and J.M. Thompson, "Neutron Diffraction Measurements of Residual Stress in Additively Manufactured Stainless Steel", *Mat. Sci. Eng. A*, vol. 678, pp. 291-298, 2016. http://dx.doi.org/10.1016/j.msea.2016.09.086
[38] Y. Ren, A. Paradowska, B. Wang, E. Eren and Y.J. Janin, "Residual Stress State of X65 Pipeline Girth Welds Before and After Local and Furnace Post Weld Heat Treatment", *J. Press. Vess. Tech.*, vol. 139(4), pp. 041401, 2017. http://dx.doi.org/10.1115/1.4035884
[39] "Mechanical Metallurgy", G.E. Dieter. Third Edition, McGraw-Hill, p. 45, 1986.
[40] M.B. Prime, R.J. Sebring, J.M. Edwards, D.J. Hughes and P.J. Webster , "Laser Surface-contouring and Spline Data-smoothing for Residual Stress Measurement", *Exp. Mech.*, vol. 44(2), pp. 176–184, 2004. https://doi.org/10.1007/BF02428177
[41] A.H. Mahmoudi and A. Saei, "Influence of asymmetrical cuts in measuring residual stresses using contour method", *Int. J. Pressure Vessels and Piping*, vol. 134,pp. 1-10, 2015. http://dx.doi.org/10.1016/j.ijpvp.2015.08.004
[42] H.F. Bueckner, The propagation of cracks and the energy of elastic deformation, *Trans. American Soc. Mech. Eng.*, vol. 80(6), pp. 1225-1230, 1958. https://doi.org/10.1016/0043-1648(59)90279-0

[43] M.D. Olson, A.T. DeWald and M.R. Hill, "Validation of a Contour Method Single-Measurement Uncertainty Estimator", *Exp. Mech.*, vol. 58(5), pp. 767-781, 2018. https://doi.org/10.1007/s11340-018-0385-4
[44] Dassault Systèmes Simulia Corp., Abaqus Analysis User's Guide version 6.14, Providence, RI, USA, 2014.
[45] R.K. Desu, H.N. Krishnamurthy, A. Balu, A.K. Gupta and S.K. Singh, "Mechanical properties of Austenitic Stainless Steel 304L and 316L at elevated temperatures", *J. Mater. Res. Technol.*, vol. 5(1), pp. 13-20, 2016. https://dx.doi.org/10.1016/j.jmrt.2015.04.001
[46] ASTM A666, "Standard Specification for Annealed or Cold-Worked Austenitic Stainless Steel Sheet, Strip, Plate, and Flat Bar", ASTM International, West Conshohocken, PA, United States, 2015. https://dx.doi.org/10.1520/A0666-15
[47] C.A. Bronkhorst, J.R. Mayeur, V. Livescu, D.W. Brown, G.T.I. Gray and S.A. Vander Wiel, "Structural representation of additively manufactured 316L austenitic stainless steel", *Int. J. Plas.*, vol. 118, pp. 70-86, 2019. https://doi.org/10.1016/j.ijplas.2019.01.012
[48] L. Ji, J. Lu, C. Liu, C. Jing, H. Fan and S. Ma, "Microstructure and mechanical properties of 304L steel fabricated by arc additive manufacturing", *MATEC Web Conf.*, vol. 128, pp. 03006, 2017. https://doi.org/10.1051/matecconf/201712803006
[49] Z. Wang, T.A. Palmer and A.M. Beese, "Effect of processing parameters on microstructure and tensile properties of austenitic stainless steel 304L made by directed energy deposition additive manufacturing", *Acta Mater.*, vol. 110, pp. 226-235, 2016. https://doi.org/10.1016/j.actamat.2016.03.019
[50] D.W. Brown, T.M. Holden, B. Clausen, M.B. Prime, T.A. Sisneros, H. Swenson and J. Vaja, "Critical Comparison of two Independent Measurements of Residual Stress in an Electron-Beam Welded Uranium Cylinder: Neutron Diffraction and the Contour Method", *Acta Mater.*, vol. 59, pp. 864-873, 2011. http://dx.doi.org/10.1016/j.actamat.2010.09.022
[51] M. Kerr, M.B. Prime, H. Swenson, M.A. Buechler, M. Steinzig, B. Clausen and T. Sisneros , "Residual Stress Characterization in a Dissimilar Metal Weld Nuclear Reactor Piping System Mock Up", *J. Pressure Vessel Technol.*, vol. 135(4), pp. 041205, 2013. http://dx.doi.org/10.1115/1.4024446
[52] P. Pagliaro, M.B. Prime, B. Clausen, M.L. Lovato and B. Zuccarello, "Known Residual Stress Specimens Using Opposed Indentation", *J. Eng. Mater. Tech.*, vol. 131, pp. 031002, 2009. http://dx.doi.org/10.1115/1.3120386
[53] M. Kartal, M. Turski, G. Johnson, M.E. Fitzpatrick, S. Gungor, P.J. Withers and L. Edwards, "Residual stress measurements in single and multi-pass groove weld specimens using neutron diffraction and the contour method", Mat. Sci. For., vols. 524-525, pp 671-676, 2006. https://doi.org/10.4028/www.scientific.net/MSF.524-525.671
[54] R. von Mises, "On Saint-Venant's Principle". *Bull. AMS*, vol. 51, pp. 555-562, 1945. https://doi.org/10.1090/S0002-9904-1945-08394-3
[55] S.P. Timoshenko and J. N. Goodier, "Theory of Elasticity," 3rd Edition, McGraw Hill, New York, 1970.
[56] M.B. Prime, A.T. DeWald, M.R. Hill, B. Clausen, M. Tran, Forensic Determination of Residual Stresses and KI from Fracture Surface Mismatch, *Eng. Fract. Mech.* 116 (2014) 158-171. https://doi.org/10.1016/j.engfracmech.2013.12.008